



MOVPE of GaN-based mixed dimensional heterostructures on wafer-scale layered 2D hexagonal boron nitride-A key enabler of III-nitride flexible optoelectronics

Suresh Sundaram, Phuong Vuong, Adama Mballo, Taha Ayari, Soufiane Karrekhou, Gilles Patriarche, Paul L Voss, Jean-Paul Salvestrini, Abdallah Ougazzaden

► To cite this version:

Suresh Sundaram, Phuong Vuong, Adama Mballo, Taha Ayari, Soufiane Karrekhou, et al.. MOVPE of GaN-based mixed dimensional heterostructures on wafer-scale layered 2D hexagonal boron nitride-A key enabler of III-nitride flexible optoelectronics. APL Materials, 2021, 9 (6), pp.061101. 10.1063/5.0049306 . hal-03350328

HAL Id: hal-03350328

<https://hal.science/hal-03350328>

Submitted on 21 Sep 2021







HAL is a multi-disciplinary open access archive for the deposit and dissemination of scientific research documents, whether they are published or not. The documents may come from teaching and research institutions in France or abroad, or from public or private research centers.

L'archive ouverte pluridisciplinaire **HAL**, est destinée au dépôt et à la diffusion de documents scientifiques de niveau recherche, publiés ou non, émanant des établissements d'enseignement et de recherche français ou étrangers, des laboratoires publics ou privés.

MOVPE of GaN-based mixed dimensional heterostructures on wafer-scale layered 2D hexagonal boron nitride—A key enabler of III-nitride flexible optoelectronics

Cite as: APL Mater. 9, 061101 (2021); <https://doi.org/10.1063/5.0049306>

Submitted: 03 March 2021 . Accepted: 10 May 2021 . Published Online: 01 June 2021

 Suresh Sundaram,  Phuong Vuong,  Adama Mballo, Taha Ayari, Soufiane Karrekhou,  Gilles Patriarche, Paul L. Voss,  Jean Paul Salvestrini,  Abdallah Ougazzaden, et al.

COLLECTIONS

Paper published as part of the special topic on [Fundamentals and Applications of Mixed-Dimensional Heterostructures](#)



View Online



Export Citation



CrossMark

ARTICLES YOU MAY BE INTERESTED IN

[One-dimensional semiconductor nanostructures grown on two-dimensional nanomaterials for flexible device applications](#)

APL Materials **9**, 060907 (2021); <https://doi.org/10.1063/5.0049695>

[Comprehensive characterization and analysis of hexagonal boron nitride on sapphire](#)

AIP Advances **11**, 055008 (2021); <https://doi.org/10.1063/5.0048578>

[Ultrawide bandgap semiconductors](#)

Applied Physics Letters **118**, 200401 (2021); <https://doi.org/10.1063/5.0055292>



A new approach to low-level measurements of nanostructures
Read our technical note

[Download Now](#)

 Lake Shore
CRYOTRONICS

MOVPE of GaN-based mixed dimensional heterostructures on wafer-scale layered 2D hexagonal boron nitride—A key enabler of III-nitride flexible optoelectronics

Cite as: APL Mater. 9, 061101 (2021); doi: 10.1063/5.0049306

Submitted: 3 March 2021 • Accepted: 10 May 2021 •

Published Online: 1 June 2021



Suresh Sundaram,^{1,2,3} Phuong Vuong,² Adama Mballo,² Taha Ayari,^{2,3} Soufiane Karrakchou,^{1,2} Gilles Patriarche,⁴ Paul L. Voss,^{1,2} Jean Paul Salvestrini,^{1,2,3} and Abdallah Ougazzaden^{1,2,a)}

AFFILIATIONS

¹ Georgia Institute of Technology School of Electrical and Computer Engineering, GT-Lorraine, 57070 Metz, France

² CNRS UMI 2958 GT-CNRS 2 Rue Marconi, 57070 Metz, France

³ GT Lorraine 2 Rue Marconi, 57070 Metz, France

⁴ Centre de Nanosciences et de Nanotechnologies, Université Paris-Saclay, C2N—Site de Marcoussis, Route de Nozay, F-91460 Marcoussis, France

Note: This paper is part of the Special Topic on Fundamentals and Applications of Mixed-Dimensional Heterostructures.

a) Author to whom correspondence should be addressed: abdallah.ougazzaden@georgiatech-metz.fr

ABSTRACT

We summarize our recent progress in Metal organic vapor phase epitaxy (MOVPE) van der Waals epitaxy of wafer-scale 2D layered hexagonal boron nitride (h-BN) on sapphire and subsequently grown III-N materials. This one step growth process allows for mechanical transfer of GaN-based devices from h-BN on sapphire to various supports. We first review the growth of h-BN on unpatterned and patterned sapphire templates. Second, we describe h-BN growth on dielectric pre-patterned sapphire templates, which enables dicing-free GaN-based device structures' pick-and-place heterogeneous integration of III-N devices. Third, we review the growth of self-assembled 1D GaN-based nanowire light emitting diode (LED) structures on layered 2D h-BN for mechanical transfer of nanowire LEDs. Together, these results illustrate the potential of wafer-scale van der Waals h-BN MOVPE to enhance the III-N device functionality and to improve III-N processing technology.

© 2021 Author(s). All article content, except where otherwise noted, is licensed under a Creative Commons Attribution (CC BY) license (<http://creativecommons.org/licenses/by/4.0/>). <https://doi.org/10.1063/5.0049306>

Hexagonal boron nitride (h-BN) is currently attracting interest for use in a wide range of electronic and optoelectronic applications.^{1–12} Due to its wide bandgap and potentially strong light emission, it can find applications in Deep ultraviolet (DUV) as an active layer, as an intrinsic p-type material, and as a photodetector.^{6–8} Due to good lattice matching with graphene, it can find application as a substrate, as protection/passivation, and as a gate dielectric in graphene electronics.⁴ Because of its layered nature, 2D–2D heterostructures with exotic properties can be formed.^{9–11} In addition to this, h-BN has a high neutron capture cross section and so finds application as efficient neutron detectors.¹² Outside of these areas, one of the most important applications of h-BN is for heterogeneous integration of III-nitride devices. This is driven by the need

for devices with flexible, stretchable, and large-area form factors for wearable devices.¹³ Compared with conventional laser or chemical lift-off processes, mechanical lift-off using hexagonal boron nitride (h-BN) as a release layer for subsequent transfer is fast, inexpensive, and non-destructive, so the substrate can be re-used, lowering cost. When compared to graphene,^{14,15} the key advantage of using layered h-BN for realizing III-nitrides is that it can be grown at wafer scale in the same reactor, even in the same epi-run with other III-nitrides. Even though there is room for improvement, considerable progress has been made in fundamental understanding of the growth of this interesting material and its emerging III-nitride device integration and lift-off. This paper summarizes recent progress in the growth of h-BN by MOVPE and realization of 3D and 1D configurations of

III-nitride device structures on h-BN/sapphire substrates and their characteristics and performances. This is especially interesting for the pick-and-place transfer process, which is useful for some key applications such as in displays and photogenetics with the need of a matrix of LEDs with different wavelengths or the integration of optoelectronic and electronic devices on silicon.

Hexagonal BN (h-BN) epitaxial layer 2" and 4" sapphire substrates were grown using a close coupled showerhead (CCS) 3×2 " MOCVD reactor using triethylboron (TEB) source and ammonia (NH_3) as boron and nitrogen precursors, respectively. The layers were grown at 1280°C in hydrogen ambient at 85 mbar. The NH_3/TEB ratio of 1000 was maintained. BN layers were grown directly on the 2" and 4" sapphire substrates with preflow of TEB but without any buffers. The TEB flow rate was $60 \mu\text{mol}/\text{min}$ for both the preflow step (5–10 s) and the BN growth step using hydrogen as the carrier gas. The total flow rate into the reactor is 20 SLPM (standard liter per minute). The growth rate of h-BN on sapphire is 15 nm/h. On patterned and reference unpatterned sapphire substrates, h-BN was grown under the same conditions. The dielectric patterns of SiO_2 and SiN were fabricated by a photolithography-based process. First, a 400 nm thick dielectric layer was deposited by plasma-enhanced chemical vapor deposition (PECVD) on a 2 in. sapphire wafer. Then, the patterns were defined by photolithography. Finally, the dielectrics were etched with hydrofluoric (HF) acid to open the device locations. Subsequently, the III-nitride device structures were grown in the same run as h-BN using standard growth conditions. Trimethyl-aluminum (TMAl), trimethyl-gallium (TMGa), trimethylindium (TMIn), and ammonia (NH_3) were used as precursors for aluminum, gallium, indium, and nitrogen, respectively. AlGaIn interfacial buffers were further used to grow GaN-based device structures. No particular limitation is seen in scaling up beyond 2" as GaN templates on hBN up to 4" have already been realized. Detailed growth conditions of the h-BN and device structures realized on h-BN can be found elsewhere.^{16–18} The crystallographic properties of the device structures on h-BN grown on patterned and unpatterned sapphire substrates were analyzed by high-resolution x-ray diffraction (HR-XRD) measurements in a Panalytical X'pert Pro Materials Research Diffractometers (MRD) system with $\text{Cu K}\alpha$ radiation. Surface morphology was analyzed by scanning electron microscopy (SEM). For the fabrication of LEDs, a standard photolithography-based process was employed. First, mesa etching isolation was achieved by inductively coupled plasma with $\text{BCl}_3/\text{Cl}_2/\text{Ar}$ chemistry. Ti/Al/Ni/Au, Ni/Au, and another Ti/Al/Ni/Au stack were used for the n-contact, the p-contact, and the pads, respectively. All the metal layers were deposited by thermal evaporation. N-contact annealing was carried out at 850°C for 30 s under N_2 ; the p-contact was annealed at 600°C for 60 s under an O_2/N_2 atmosphere. Dark I–Vs was measured by an automated probe station. Resist development, resist stripping, and metal lift-off step were performed with gentle agitation of the liquids to limit the delamination risk.

MOCVD growth of large-area h-BN layers with high structural quality and uniform morphology has been reported by our group.^{16–18} A topographic transition of BN thin layers has been observed, as shown in Fig. 1. SEM images of the BN samples show that it is atomically flat up to a thickness less than 10 nm and develops surface pleats with increasing thickness. However, the atomic force microscope (AFM) images show pleat formation on the surface

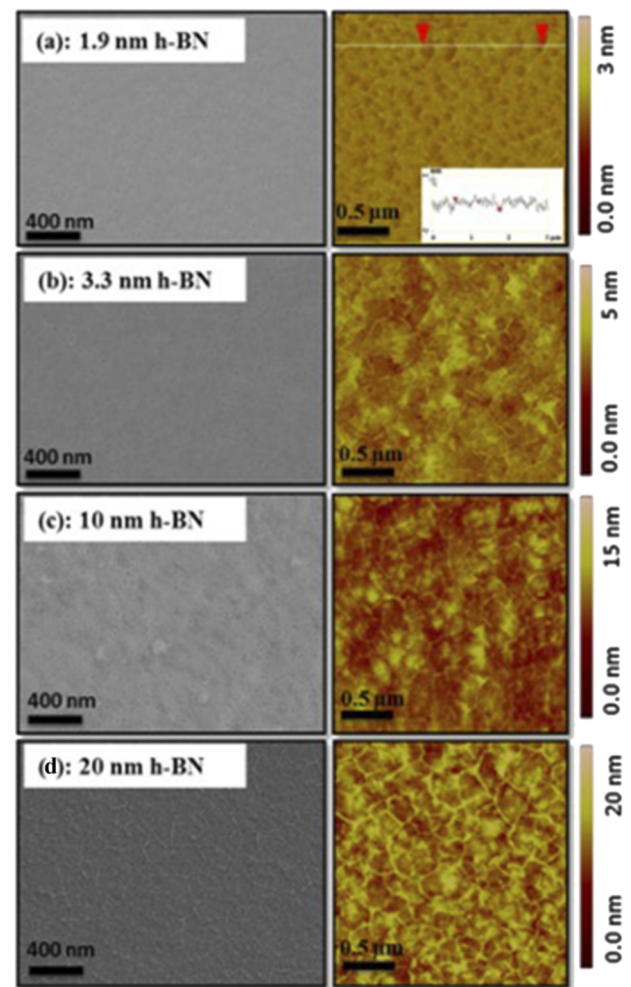


FIG. 1. SEM (on the left) and AFM (on the right) images of h-BN with different thicknesses: (a) 1.9 nm, (b) 3.3 nm, (c) 10 nm, and (d) 20 nm.

of the h-BN samples above 3 nm thick [Figs. 1(b)–1(d), right panels]. These pleats are characteristics of 2D materials and are now important in determining the quality of the grown material.^{16,19–24} We observe that the rms roughness values increase linearly from 0.2 to 3 nm with h-BN thickness. To analyze the continuity of the thinnest (1.9 nm thick) h-BN layer, the line scan from the AFM image [the inset of Fig. 1(a)] was further examined. The extracted maximum depths of the pits are less than 1 nm, which are much lower than the total thickness of the h-BN layer, confirming that the h-BN layer is continuous on a sapphire substrate. The continuity of the h-BN layer is important for avoiding direct seeding of III-nitrides or other heteronuclei on sapphire substrates, which may hinder complete lift-off of the grown layer.²⁵

The Raman spectrum of the thin BN film clearly displayed a peak at 1370 cm^{-1} that is attributed to the h-BN first-order Raman E_{2g} vibrational mode.^{26–28} The variation of the full width at half maximum (FWHM) of the peak and the peak position with respect to the thickness of the layer is plotted and is shown in Fig. 2. The

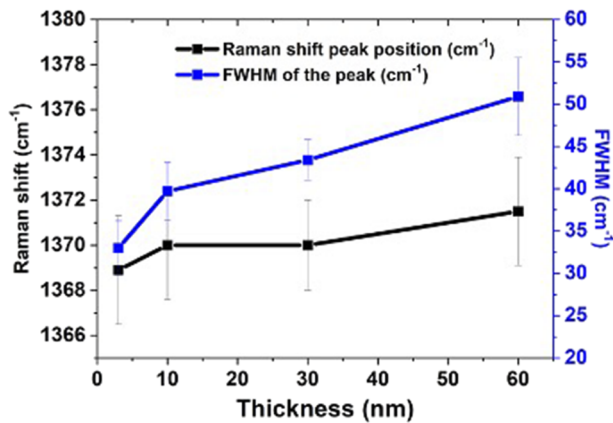


FIG. 2. Raman peak position and peak full width at half maximum (FWHM) of h-BN with different thicknesses of h-BN.

peak FWHM varies from 34 to 52 cm^{-1} on increasing the thickness from 3 to 60 nm. These FWHM values are comparable with those observed for single crystal BN flakes fabricated by MBE²⁹ and by CVD.³⁰ Very narrow FWHM was also reported in the literature for bulk h-BN (11.7 cm^{-1}) or few layer h-BN flakes (15.6 cm^{-1}).²⁶ The relatively broad peak obtained here might be caused by the spatial strain variation in the layer. Non-uniform strain would split the E_{2g} peak as has been observed for other 2D materials,^{31–33} leading to a broader peak. In particular, for 2-in. wafer-scale continuous thin films on a substrate, the thermal strain from the cooling process after the epitaxial growth cannot be effectively released. The pattern of the pleats presented in the morphology studies is also related to the localized strain in the layer. The strain variation across the pleats produces phonon shifts and, hence, Raman peak dispersion.^{34–36} A further increase in the thickness of the h-BN layers leads to the formation of misoriented islands of h-BN or turbostratic insertions with thickness and then complete transformation to 3D turbostratic BN.^{21,37}

High-resolution transmission electron microscopy (HR-TEM) reported elsewhere confirmed that these thin layers of BN are layered.^{16–18} A further study of the stacking sequence also confirmed that the layered structure is hexagonal. In addition, cross-sectional scanning transmission electron microscopy (STEM) is used to explain the origin of these surface pleats. Thin layer buckling occurs in order to release the thermal compression energy that is generated during cooling. In the pleated area, the stacks of the as-grown basal planes are still highly oriented, but they are bent following the pleats' waviness. The local decohesion of the h-BN layer was also observed at the maximum height of a pleat. The local decohesion could be caused by the weaker van der Waals forces between h-BN and the substrate in this area due to the direct growth on the sapphire substrate without any 3D bonded nucleation/buffer layers. Recently, different high-quality GaN-based device structures, such as InGaN and AlGaN light emitting diodes (LEDs) and high electron mobility transistors (HEMTs), were grown on h-BN, and the transfer to arbitrary substrates has been demonstrated.^{18,38,39} GaN on BN was structurally similar to GaN on graphene reported elsewhere,¹⁵ and the total threading dislocation density was around

$1 \times 10^9 \text{ cm}^{-2}$. The quality of GaN is improved by reducing the h-BN thickness. The minimum thickness is limited by the entire coverage of the sapphire surface. In our growth conditions, the minimum thickness is around 1 nm. These experiments showed that by a suitable choice of the support receiving the substrate, device operating temperature may be raised, leading to more efficient gas detection, or lowered, leading to the lower temperature operation of LEDs.

At the same time, it may be possible to better reduce potential delamination. Controlling the stress induced decohesion and its evolution in h-BN may lead to many reliable and reproducible applications, especially in the van der Waals epitaxial growth of the other III-nitrides where self-delamination during growth and delamination during the front-end process are reported and seen as serious issues. To attempt to control and to study its evolution and characteristics, h-BN was grown on patterned sapphire substrates. It is worth noting that, generally, the growth of III-nitrides at a relatively higher temperature may be before the evolution of the surface pleats on thin h-BN.

A first attempt to grow h-BN on patterned substrates resulted in h-BN grown on sub-micrometer-sized dome patterned sapphire substrates. BN covered both the *c*-plane and the domes uniformly. A typical pleated surface of h-BN was observed on *c*-plane sapphire, confirming that this h-BN is crystalline and layered. More pleats of h-BN were formed on the domes. Detailed structural studies using HR-TEM on these areas showed that h-BN continuously covers the domes like a blanket of snow. At the intersections of the domes and the *c*-plane, strain generated stacking faults and few h-BN islands were seen, evidence of strain localization induced by the misorientations. This study suggested that it could be possible to achieve local control of the structural and optical characteristics of h-BN.²³

Better control was anticipated if dielectric patterned sapphire substrates with different geometries were utilized. Hence, high-quality thicker h-BN layers were grown on dielectric patterned sapphire substrates. As expected, on the un-patterned area, h-BN formed semi-hexagonal pleats, which matched the quality of standard high-quality h-BN, as shown in SEM images of Fig. 3(a). BN deposits on the dielectric region were difficult to detect. However, the presence of BN on the dielectric patterns was identified and confirmed with localized SIMS measurements and found to be of comparable thickness to h-BN on the un-patterned area. As the thickness was comparable, we conclude that h-BN growth under this growth condition is non-selective. Further cross-sectional TEM studies on the samples are shown in Figs. 3(b) and 3(c). BN on SiO_2 presented a layered structure when compared to BN on *c*-plane sapphire. However, the fast Fourier transform (FFT) pattern of this high-resolution TEM image shown in Figs. 3(d) and 3(e) clearly showed the differences between these layers. It gave a diffused ring pattern for BN on SiO_2 , indicating that this BN has only a short-range order, whereas BN on *c*-plane sapphire displayed diffraction spots corresponding to the hexagonal structure of BN, confirming that they are completely crystalline. This demonstrates that h-BN grows non-selectively, but there is a radical difference in quality between BN on dielectric SiO_2 and on sapphire substrates, which can be exploited for growing selectively III-nitride device structures.

Subsequently, III-nitride device structures were grown on h-BN on patterned sapphire substrates along with control samples. These

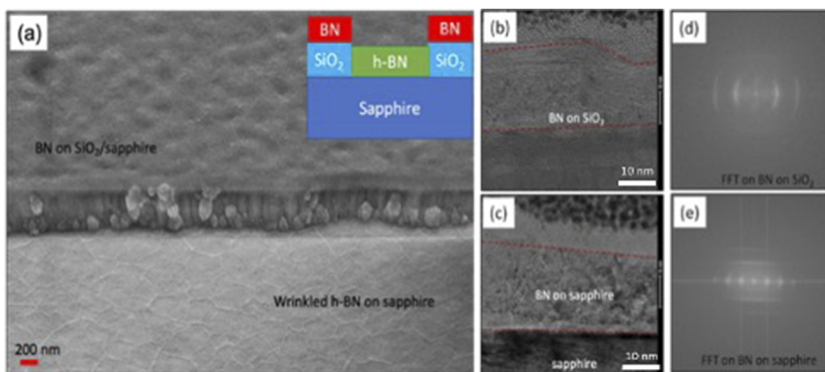


FIG. 3. (a) Top-view SEM image of BN on SiO₂ dielectric patterns and on c-plane sapphire along with the cross section of the structure in the inset. [(b) and (c)] HR-TEM images of BN deposits on the SiO₂ pattern and c-plane sapphire, respectively. The scale bar is 10 nm. FFT patterns [(d) and (e)] captured from the area shown in (b) and (c), respectively, indicate that BN on SiO₂ is nanocrystalline, whereas BN on c-plane sapphire is perfectly crystalline.

samples were characterized to study the selectivity of III-nitrides. To study the structural characteristics of these device structures, non-destructive XRD measurements were made on the sample on h-BN templates. High-Resolution X-ray Diffraction (HR-XRD) 2θ - ω scans of five period InGa_{0.14}N/GaN blue LEDs on h-BN on SiO₂ and SiN patterned sapphire substrates in comparison with h-BN on unpatterned sapphire substrates are shown in Fig. 4. This measured scan is similar to the one reported previously and is comparable with our standard LED on sapphire.¹⁸

The XRD scans clearly presented the MQW satellite peaks up to the fourth order and the peaks from the GaN and Al_{0.14}Ga_{0.86}N layers, confirming high interface quality in the InGa_{0.14}N/GaN MQW structure. Comparing the measured scans on the unpatterned sample to scans of the patterned, it can be observed that there is no considerable peak shift or peak broadening, which further confirms that the patterning process does not affect the structural quality of LEDs on BN. This is unexpected because the van der Waals epitaxial growth of boron nitride is not likely completely selective since it is theoretically substrate independent growth. On the other hand, the quality of BN on randomly oriented SiO₂ patterns may be significantly different when compared to h-BN on highly oriented c-plane sapphire since the substrate orientation controls the quality of these van der Waals layers.^{23,40} This cross-quality BN on SiO₂ patterns should lead to non-uniform III-nitride growth due to the difference in surface growth kinetics that may alter the XRD

scans unless otherwise the GaN device structures are growing selectively avoiding BN on SiO₂. To first confirm these insights, surface morphology of the GaN LEDs on patterned samples was studied with SEM.

The SEM image in Fig. 5(a) vividly shows the selective growth of the GaN-based LED structure in regions where layered h-BN is deposited, avoiding the growth on randomly oriented BN on SiO₂. The higher magnification SEM image shown in Fig. 5(b) depicts a clear boundary and very sharp side walls of the LED structure in each side of the mask, which are required to guarantee the separation between the devices after the fabrication process. It is also observed from other higher magnification images shown in Fig. 5(c) that there are some nanocrystalline deposits on the surface of the SiO₂ masks, which can be cross-quality BN and other polycrystalline material deposits of III-nitride. Similar selectivity has also been observed in SiN patterned sapphire substrates.

Following this study, a full front-end lithography, etching, and metal deposition process was applied on the LED wafer to create devices on the as-grown wafer, as shown in Fig. 6(a). Thanks to the patterning with the SiO₂ mask, the fabricated devices are already physically isolated from each other. The discrete LEDs can be released and transferred individually without the need for a dicing step. In this work, a particular set of devices has been released from the matrix of processed devices by means of a water-dissolvable tape and transferred to a flexible aluminum tape. The mechanical exfoliation transfer process is relatively fast (only takes few seconds) after pressing the tape on the layer for proper contact, and peel off involves shear force on the interface. The water-dissolvable tape has a 20 μ m thick adhesive layer on it.^{41,42} The tape is attached to a carrier for the release. Then, once the device is placed on the final support platform, the tape is simply removed by dissolving it in water for around 1 min. The pick-and-place capability is demonstrated in Fig. 7(a) where we clearly see that specific aimed devices have been lifted off from sapphire, leaving their locations empty, while other untargeted LEDs remained on the growth wafer. During the transfer process, device structures remained completely intact and free from cracks and metallic contact damage. I-V measurements for the released LEDs were performed after its transfer to confirm the preservation of the device functionality, as shown in Fig. 7(b), and the inset of Fig. 7(b) shows a photograph of the blue light emission from the LED after its release from the substrate and transfer to the aluminum tape.

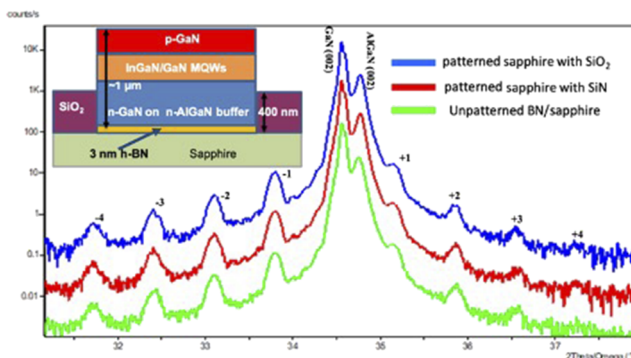


FIG. 4. HR-XRD 2θ - ω scans measured from GaN-based blue LEDs on h-BN grown on patterned and unpatterned sapphire templates.

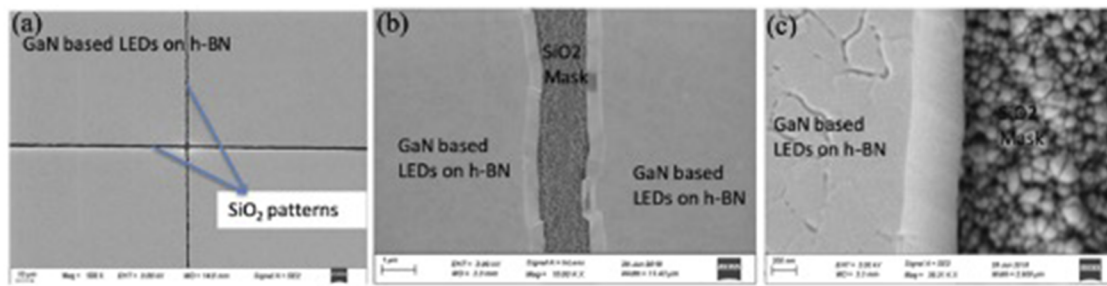


FIG. 5. SEM image of the surface of InGaN-based blue LEDs grown on SiO_2 patterned h-BN templates in various magnifications (a) 500X, (b) 10 KX, and (c) 39.31 KX, clearly showing a selective epitaxial lateral growth of GaN device structures on h-BN on c-plane sapphire substrates only.

The growth of 1D nitride device structures on h-BN is also possible by self-assembly on layered BN. h-BN was first grown after nitridation and surface smoothing by AlN deposition on sapphire substrates since the direct growth of GaN resulted in the formation of sparsely distributed isolated discrete polycrystalline GaN lumps.¹³ Uniform nucleation on dangling bond-free h-BN was induced using short pulse of AlN growth before successive GaN growth. AlN islands on h-BN serve as nucleation sites for the uniform growth of GaN. Immediately after AlN nucleation, GaN was grown under conventional GaN growth conditions, forming vertical GaN nanorods. Figure 8(a) shows the tilted scanning electron microscopy (SEM) image of the formed GaN nanorod arrays with the hexagonal sixfold arrangement of the wurtzite lattice structure on sapphire substrates. The inset of Fig. 8(a) shows the cross-sectional SEM image of the GaN nanorods, confirming vertical alignment. This first growth of GaN nanorods on layered h-BN in a single step with wafer-scale uniformity is the result of the combination of the van der Waals epitaxial growth of the h-BN layer and nanoseeding of crystals by AlN. We note that control over the density and aspect ratio of the GaN nanorods can be achieved by adjusting the density and size of the AlN islands on h-BN. Islands of varying sizes and densities were grown by changing the AlN growth time on 2D h-BN, after which the GaN nanorods were grown. As the AlN nucleation layer growth time increases, the nanorod density increases almost linearly and the size of the rods decreases. The variation of nucleation density and the average size with respect to the AlN seeding or nucleation layer

growth time is shown in Fig. 8(b). An increase in the nucleation density beyond a certain limit (18 s of AlN growth) resulted in coalesced GaN nanorod structures increasing in size.

Having established the high-quality growth and control of GaN nanowires' dimension and density on h-BN templates, the feasibility of growing nanodevice structures on 2D layered h-BN was explored. PIN nanodevice structures as shown in the inset of Fig. 9(a) were grown. The initial GaN nanorod on h-BN buffered sapphire templates was doped with silane to form an n-type rod. In addition to this, nanostructures, InGaN layers, and p-GaN layers with Mg doping were added on top of it. Figure 9(a) shows the low magnification tilted view SEM image of the resulting p-GaN/i-InGaN/n-GaN PIN nanodevices. Figure 9(b) shows the cross-sectional high magnification image of a few PIN nanodevice structures on the AlN/h-BN buffered sapphire substrates. These nanoLED structures are uniform in shape with flat top and have the hexagonal sixfold arrangement, confirming the single crystalline wurtzite lattice structure. Even though the p-GaN/i-InGaN/n-GaN PIN device structures were grown on layered h-BN, the hexagonal shape of these nanorod-based structures is similar to those of GaN nano- and microrods reported on single crystal substrates.^{43–45} We envision that the tilt component of the nanorods structures can be further controlled by improving the quality of the AlN nucleation layer and h-BN layer. Under electrical injection, the PIN nanodevice structures emitted blue light, as shown in Fig. 9(c), which demonstrates the full functionality of the as-grown nanodevice structures. The formation of the core-shell structure and the presence of the h-BN were confirmed by high-resolution cross-sectional transmission electron microscope studies and reported separately elsewhere.⁴⁶

Nanorods on a 2 in. sapphire substrate were then lifted off by a simple mechanical peeling technique using a copper tape. After tapping the surface of nanorods, the tape was peeled off holding the sapphire substrates, which prompted a shear stress at the nanorods/h-BN interfaces separating them. The SEM images of the top surface of the lifted-off planarized nanorods in the Cu metallic tape are shown in Figs. 10(a) and 10(b). The SEM image clearly displays damage-free bases of the nanorods with flat surfaces and no visible breakage or cracks on the nanorod structures. Backside surfaces of the nanorods are smooth and similar to the surface of h-BN covered with misoriented AlN or AlGaIn islands with some nanovoids on it, which further confirms that the lift-off occurred at the h-BN/sapphire interfaces. This simple mechanical exfoliation technique allows for the

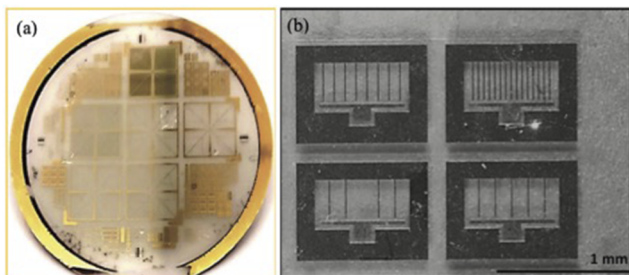


FIG. 6. (a) Photograph and (b) optical microscope image of devices with a 1 mm^2 contact area of the full front-end processed GaN-based blue LEDs on h-BN grown on patterned sapphire templates. Source: Ayari *et al.*⁴²

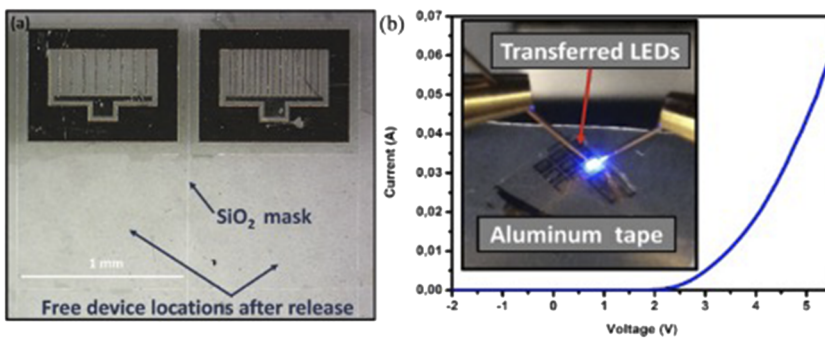


FIG. 7. (a) Optical microscope images showing two LEDs with a 1 mm² contact area and empty locations of two lifted-off LEDs on h-BN grown on the patterned sapphire, demonstrating patterning induced isolation and specific device lift-off. (b) I-V characteristics of a device after its transfer with its blue light emission shown in the inset. Source: Ayari *et al.*⁴²

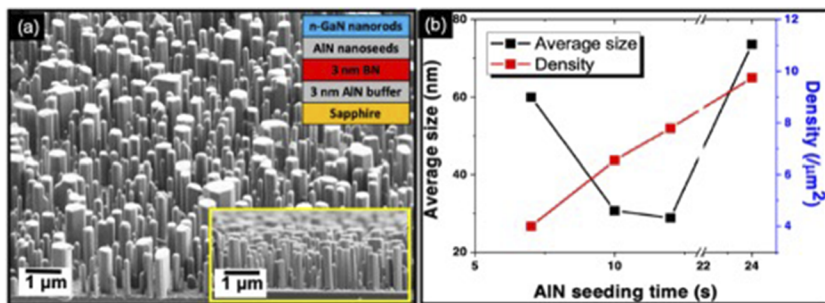


FIG. 8. SEM images. (a) Tilted view of the GaN nanorod structure on the sapphire substrates with a clear hexagonal symmetry, and the inset shows a higher magnification cross-sectional view of the GaN nanostructures vividly displaying the vertical alignment. (b) Variation of nucleation density and average size (diameter) of GaN nanorods with AlN seeding time. Source: Sundaram *et al.*⁴⁶

transfer of the nanorods to any appropriate platform without any interface damage, preserving structural and optical quality. Even though BN is highly resistive, the sacrificial layer is very thin; hence, the carriers are expected to tunnel through them. If required, this thin layer can be removed completely using a smooth dry etch process right after the lift-off step so that bottom Ohmic contact to GaN nanowires can be formed without any issues in both cases. In addition, combining dielectric patterning and growing GaN nanowires on BN with GaN self-nucleation may lead to the position-controlled growth of nanowires that can, consequently, result in addressable integrated/active-matrix devices.

In summary, significant progress in the MOCVD growth of GaN-based device structures on h-BN epilayers has been made.

The modified front-end process applied to device structures on h-BN on the patterned sapphire substrate showed continued operation without degradation of the structural integrity of the layers. A dramatic self-assembly of GaN nanorods and nanoLED structures' growth was also demonstrated with blue light emission. Both of these approaches improve the GaN material quality by reducing threading dislocation density and associated issues and by avoiding self-delamination occurring during the growth and front-end process. We have also demonstrated III-nitride device structures on BN on patterned templates with *in situ* device isolation and self-assembled nanoLEDs, which allowed for the smooth, crack-free, and interface damage-free mechanical release of specific pixel from the matrix. The characterization performed on the transferred device

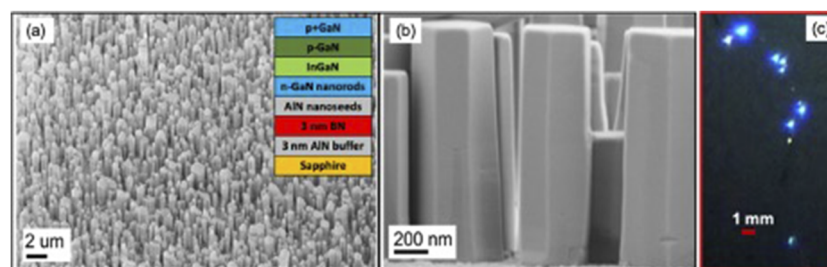


FIG. 9. SEM image of (a) p-GaN/i-InGaN/n-GaN nano-PIN structures on h-BN/sapphire substrates, and the inset shows the designed structure. (b) High magnification cross-sectional SEM image of nano-PIN on the h-BN/sapphire substrates showing the vertical alignment and flat-topped hexagonal columns of the nanorods and (c) blue light emission from the nano-PIN structure under electrical injection. Source: Sundaram *et al.*⁴⁶

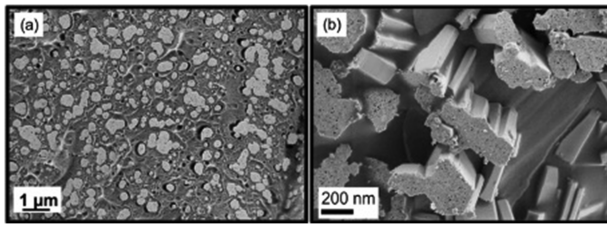


FIG. 10. (a) Lifted-off core-shell nanorods using the copper tape (bottom view) and (b) higher magnification SEM image, confirming the retention of the core-shell nanorods after the lift-off. Source: Sundaram *et al.*⁴⁶

structures after lift-off showed that the structural, optical, and electrical functionalities of the devices have been preserved, which is interesting for realizing pick-and-place assembly technology, which suits the next generation highly efficient and flexible opto-electronic devices.

This study was partially funded by the French National Research Agency (ANR) under the GANEX Laboratory of Excellence (Labex) project. The authors also acknowledge all staff members of Institute Lafayette, France, for extending facilities and support for processing the samples. G.P. acknowledges the French National Research Agency for the project TEMPOS (Grant No. ANR-10-EQPX-50) in the framework of the “Future Investments” program.

DATA AVAILABILITY

The data that support the findings of this study are available from the corresponding author upon reasonable request.

REFERENCES

- ¹C. R. Dean, A. F. Young, I. Meric, C. Lee, L. Wang, S. Sorgenfrei, K. Watanabe, T. Taniguchi, P. Kim, K. L. Shepard, and J. Hone, *Nat. Nanotechnol.* **5**, 722–726 (2010).
- ²J. Li, S. Majety, R. Dahal, W. P. Zhao, J. Y. Lin, and H. X. Jiang, *Appl. Phys. Lett.* **101**, 171112 (2012).
- ³Z. Xu, R. Zheng, A. Khanaki, Z. Zuo, and J. Liu, *Appl. Phys. Lett.* **107**, 213103 (2015).
- ⁴S. Vangala, G. Siegel, T. Prusnick, and M. Snure, *Sci. Rep.* **8**, 8842 (2018).
- ⁵G. Cassabois, P. Valvin, and B. Gil, *Nat. Photonics* **10**, 262–266 (2016).
- ⁶A. Mballo, A. Srivastava, S. Sundaram, P. Vuong, S. Karakchou, Y. Halfaya, S. Gautier, P. L. Voss, A. Ahaitouf, J. P. Salvestrini, and A. Ougazzaden, *Nanomaterials* **11**, 211 (2021).
- ⁷R. Dahal, J. Li, S. Majety, B. N. Pantha, X. K. Cao, J. Y. Lin, and H. X. Jiang, *Appl. Phys. Lett.* **98**, 211110 (2011).
- ⁸D. A. Laleyan, S. Zhao, S. Y. Woo, H. N. Tran, H. B. Le, T. Szkopek, H. Guo, G. A. Botton, and Z. Mi, *Nano Lett.* **17**, 3738–3743 (2017).
- ⁹A. K. Geim and I. V. Grigorieva, *Nature* **499**, 419–425 (2013).
- ¹⁰S. Jaewoo, S.-H. Bae, W. Kong, D. Lee, K. Qiao, D. Nezich, Y. J. Park, R. Zhao, S. Sundaram, X. Li, H. Yeon, C. Choi, H. Kum, R. Yue, G. Zhou, Y. Ou, K. Lee, J. Moodera, X. Zhao, J. Hyun, A. Ougazzaden, and J. Kim, *Science* **362**, 665 (2018).
- ¹¹J. Gigliotti, X. Li, S. Sundaram, D. Deniz, V. Prudkovskiy, J.-P. Turmaud, Y. Hu, Y. Hu, F. Fossard, J.-S. Mérot, A. Loiseau, G. Patriarche, B. Yoon, U. Landman, A. Ougazzaden, C. Berger, and W. A. de Heer, *ACS Nano* **14**, 12962 (2020).

- ¹²A. Maity, S. J. Grenadier, J. Li, J. Y. Lin, and H. X. Jiang, *J. Appl. Phys.* **123**, 044501 (2018).
- ¹³Y. Kobayashi, K. Kumakura, T. Akasaka, and T. Makimoto, *Nature* **484**, 223 (2012).
- ¹⁴K. Chung, C.-H. Lee, and G.-C. Yi, *Science* **330**, 655 (2010).
- ¹⁵J. Kim, C. Bayram, H. Park, C. W. Cheng, C. Dimitrakopoulos, J. A. Ott, K. B. Reuter, S. W. Bedell, and D. K. Sadana, *Nat. Commun.* **5**, 4836 (2014).
- ¹⁶X. Li, S. Sundaram, Y. El Gmili, T. Ayari, R. Puybaret, G. Patriarche, P. L. Voss, J. P. Salvestrini, and A. Ougazzaden, *Cryst. Growth Des.* **16**, 3409 (2016).
- ¹⁷S. Sundaram, X. Li, S. Alam, T. Ayari, Y. Halfaya, G. Patriarche, P. L. Voss, J. P. Salvestrini, and A. Ougazzaden, *J. Cryst. Growth* **507**, 352–356 (2019).
- ¹⁸T. Ayari, S. Sundaram, X. Li, Y. El Gmili, P. L. Voss, J. P. Salvestrini, and A. Ougazzaden, *Appl. Phys. Lett.* **108**, 171106 (2016).
- ¹⁹Y. Kobayashi and T. Akasaka, *J. Cryst. Growth* **310**, 5044–5047 (2008).
- ²⁰Q. Paduano, M. Snure, D. Weyburne, A. Kiefer, G. Siegel, and J. Hu, *J. Cryst. Growth* **449**, 148–155 (2016).
- ²¹D. Chugh, J. Wong-Leung, L. Li, M. Lysevych, H. H. Tan, and C. Jagadish, *2D Mater.* **5**, 045018 (2018).
- ²²X. Yang, S. Nitta, M. Pristovsek, Y. Liu, K. Nagamatsu, M. Kushimoto, Y. Honda, and H. Amano, *Appl. Phys. Express* **11**, 051002 (2018).
- ²³S. Sundaram, X. Li, S. Alam, Y. Halfaya, G. Patriarche, and A. Ougazzaden, *J. Cryst. Growth* **509**, 40–43 (2019).
- ²⁴A. K. Dąbrowska, M. Tokarczyk, G. Kowalski, J. Binder, R. Božek, J. Borysiuk, R. Stepniowski, and A. Wyszomolek, *2D Mater.* **8**, 015017 (2020).
- ²⁵W. Kong, H. Li, K. Qiao, Y. Kim, K. Lee, Y. Nie, D. Lee, T. Osadchy, R. J. Molnar, D. K. Gaskill, R. L. Myers-Ward, K. M. Daniels, Y. Zhang, S. Sundram, Y. Yu, S.-h. Bae, S. Rajan, Y. Shao-Horn, K. Cho, A. Ougazzaden, J. C. Grossman, and J. Kim, *Nat. Mater.* **17**, 999–1004 (2018).
- ²⁶L. Song, L. Ci, H. Lu, P. B. Sorokin, C. Jin, J. Ni, A. G. Kvashnin, D. G. Kvashnin, J. Lou, B. I. Yakobson, and P. M. Ajayan, *Nano Lett.* **10**, 3209–3215 (2010).
- ²⁷R. Geick, C. H. Perry, and G. Rupprecht, *Phys. Rev.* **146**, 543–547 (1966).
- ²⁸S. Reich, A. C. Ferrari, R. Arenal, A. Loiseau, I. Bello, and J. Robertson, *Phys. Rev. B* **71**, 205201 (2005).
- ²⁹Z. Zuo, Z. Xu, R. Zheng, A. Khanaki, J.-G. Zheng, and J. Liu, *Sci. Rep.* **5**, 14760 (2015).
- ³⁰R. Y. Tay, M. H. Griep, G. Mallick, S. H. Tsang, R. S. Singh, T. Tumlin, E. H. T. Teo, and S. P. Karna, *Nano Lett.* **14**, 839–846 (2014).
- ³¹T. M. G. Mohiuddin, A. Lombardo, R. R. Nair, A. Bonetti, G. Savini, R. Jalil, N. Bonini, D. M. Basko, C. Galiotis, N. Marzari, K. S. Novoselov, A. K. Geim, and A. C. Ferrari, *Phys. Rev. B* **79**, 205433 (2009).
- ³²H. J. Conley, B. Wang, J. I. Ziegler, R. F. Haglund, S. T. Pantelides, and K. I. Bolotin, *Nano Lett.* **13**, 3626–3630 (2013).
- ³³M. A. Bissett, M. Tsuji, and H. Ago, *Phys. Chem. Chem. Phys.* **16**, 11124–11138 (2014).
- ³⁴A. Castellanos-Gomez, R. Roldán, E. Cappelluti, M. Buscema, F. Guinea, H. S. J. Van Der Zant, and G. A. Steele, *Nano Lett.* **13**, 5361–5366 (2013).
- ³⁵I. Polyzos, M. Bianchi, L. Rizzi, E. N. Koukaras, J. Parthenios, K. Papagelis, R. Sordan, and C. Galiotis, *Nanoscale* **7**, 13033–13042 (2015).
- ³⁶W. Zhu, T. Low, V. Perebeinos, A. A. Bol, Y. Zhu, H. Yan, J. Tersoff, and P. Avouris, *Nano Lett.* **12**, 3431–3436 (2012).
- ³⁷X. Li, M. B. Jordan, T. Ayari, S. Sundaram, Y. El Gmili, S. Alam, M. Alam, G. Patriarche, P. L. Voss, J. Paul Salvestrini, and A. Ougazzaden, *Sci. Rep.* **7**, 786 (2017).
- ³⁸T. Ayari, C. Bishop, M. B. Jordan, S. Sundaram, X. Li, S. Alam, Y. ElGmili, G. Patriarche, P. L. Voss, J. P. Salvestrini, and A. Ougazzaden, *Sci. Rep.* **7**, 15212 (2017).
- ³⁹T. Ayari, S. Sundaram, X. Li, S. Alam, C. Bishop, W. El Huni, M. B. Jordan, Y. Halfaya, S. Gautier, P. L. Voss, J. P. Salvestrini, and A. Ougazzaden, *ACS Photonics* **5**, 3003 (2018).

- ⁴⁰X. Zhang, T. H. Choudhury, M. Chubarov, Y. Xiang, B. Jariwala, F. Zhang, N. Alem, G.-C. Wang, J. A. Robinson, and J. M. Redwing, *Nano Lett.* **18**, 1049–1056 (2018).
- ⁴¹S. Karrakchou, S. Sundaram, T. Ayari, A. Mballo, P. Vuong, A. Srivastava, R. Gujrati, A. Ahaitouf, G. Patriarche, T. Leichlé, S. Gautier, T. Moudakir, P. L. Voss, J. P. Salvestrini, and A. Ougazzaden, *Sci. Rep.* **10**, 21709 (2020).
- ⁴²T. Ayari, S. Sundaram, C. Bishop, A. Mballo, P. Vuong, Y. Halfaya, S. Karrakchou, S. Gautier, P. L. Voss, J. P. Salvestrini, and A. Ougazzaden, *Adv. Mater. Technol.* **4**, 1900164 (2019).
- ⁴³X. Dai, A. Messanvi, H. Zhang, C. Durand, J. Eymery, C. Bougerol, F. H. Julien, and M. Tchernycheva, *Nano Lett.* **15**, 6958 (2015).
- ⁴⁴Q. Li, J. B. Wright, W. W. Chow, T. S. Luk, I. Brener, L. F. Lester, and G. T. Wang, *Opt. Express* **20**, 17873 (2012).
- ⁴⁵K. Chung, H. Beak, Y. Tchoe, H. Oh, H. Yoo, M. Kim, and G.-C. Yi, *APL Mater.* **2**, 092512 (2014).
- ⁴⁶S. Sundaram, X. Li, Y. Halfaya, T. Ayari, G. Patriarche, C. Bishop, S. Alam, S. Gautier, P. L. Voss, J. P. Salvestrini, and A. Ougazzaden, *Adv. Mater. Interfaces* **6**, 1900207 (2019).